AIMS Bioengineering

AIMS Bioengineering, 13(1): 96–114.
DOI: 10.3934/bioeng.2026005
Received: 01 December 2025
Revised: 07 February 2026
Accepted: 24 February 2026
Published: 06 March 2026

https://www.aimspress.com/journal/Bioengineering

Research article

Optical and embedded ML driven computational optimization of portable micro-volume spectrophotometer for biochemical analysis in resource-limited environment

Abia Moiz*, Ayesha Faiz Ur Rasool, Muhammad Aamir and Irfan Ahmed Usmani

Department of Biomedical Engineering, Salim Habib University, NC-24, Deh Dih, Salim Habib Road, Karachi, 74900, Pakistan

* **Correspondence:** Email: s23bme006@shu.edu.pk; Tel: +923334053947.

Abstract: Comprehensive biochemical analysis is an essential part of clinical diagnostics, pharmaceutical development, and biomedical research. The gold-standard technique for such analysis is spectrophotometry, which has demonstrated excellent reliability, quantitative accuracy, and broad biomolecular sensitivity. Commercial micro-volume spectrophotometers, which are instrumental to applications with limited sample volumes, are often restricted to well-equipped laboratories due to the high cost and portability limitations especially in resource-limited settings. To address this gap, we propose a proof-of-concept, 3D-printed micro-volume spectrophotometer that integrates precision optics, microfluidic sample handling (8–15 µL), combined with spectral reconstruction and machine learning-based concentration estimation algorithm in a compact and affordable format. Preliminary validation of the proposed system based on bovine serum albumin (BSA) protein quantification via Biuret assay demonstrates strong agreement with commercial spectrophotometers ($R^2 > 0.91$). With a production cost of approximately $36 and rapid measurement, the architecture provides a framework that can be extended to other absorbance-based biochemical assays ensuring accessible spectrophotometric systems for point-of-care and resource-limited applications, overcoming traditional limits of cost, sample volume, and portability.

Keywords: tiny ML; portable spectrophotometry; regression AI; embedded neural networks; point of care devices; optoelectronics

1. Introduction

Spectroscopy is among the most common methods of analysis extensively used by the scientific community to measure the quantitative level of light-absorbing substances in a sample. This technique is naturally regulated by the Beer-Lambert law, which creates a linear correlation between absorbance, solute concentration and optical path lengths.

The spectrophotometers designed for cuvettes require macro volume samples, as they use the standard 10 mm cuvette [1]. Common benchtop instruments (e.g., Thermo Scientific GENESYS 150 UV-Vis Spectrophotometer and Jenway 73-series) generally use 1–3 mL sample volumes [2] which results in significant waste of valuable or scarce biological sample [3]. This aspect makes them unfit for use with precious or water-scarce biological samples.

This has led to the creation of micro-volume spectrophotometers, such as NanoDrop by ThermoFisher, which has transformed the way samples are analyzed by utilizing microliter scale volumes as small as 0.5–2 µL [4]. These tools have great benefits, such as higher sensitivity, better efficiency while handling, and fast, non-destructive measurement, which is essential to the preservation of invaluable material in the realms of genomics and forensics [5].

The ability to scale downstream applications (such as PCR, quantitative PCR [qPCR] and next-generation sequencing [NGS]) on minute quantities of DNA and RNA is particularly essential where original biological samples are limited, and conventional PCR technology is either prohibitively expensive or unavailable [6]. These limitations are typical in pharmaceutical applications, where non-destructive concentration analysis of drugs may be performed using spectrophotometry, such as volume-sensitive assays, pediatric preparations, orphan drugs, and other micro-dose therapies. Likewise, micro-volume spectrophotometry is a key component of the current study, and protein quantification, a vital application of micro-volume spectrophotometry, required in a variety of biochemical and biotechnological research, such as enzyme assays, Western blotting, and drug-protein interaction studies [7].

In addition to micro-volume assessment, there is an increasing need to have portable and cost-effective instrumentation that will allow on-site and field testing to be performed alongside real-time analysis for instant decision making with minimal logistical hassle and expenses involved in carrying samples to centralized labs. Recent improvements in handheld instruments like ThermoScientific Eutech and Hach DR1900 Portable Spectrophotometers have shown to be reliable in environmental and biochemical analysis in the field with little power consumption and reagent volumes [8]. Another example of the tendency of miniaturization is in the new smartphone-based optical systems [9,10]. These innovations contribute to the shift to resource-efficient, point-of-care analytical systems that are able to expand biochemical quantification beyond traditional, centralized laboratory systems. While these systems provide accurate and reproducible measurements, their cost and form factor restrict widespread adoption, motivating the development of low-cost alternatives in micro-volume spectrophotometry.

Photodiodes or CMOS sensors are used in the commercially available spectrophotometers. CMOS provides compact, fast, and integrated solutions to miniaturized instruments. Light sources may be wide-spectrum with high brightness xenon and deuterium lamps that are usually expensive and prone to variations [11] or energy-saving, portable, and low-cost LEDs. Although LEDs might have a more limited wavelength range than more traditional sources, their intrinsic benefits allow them to be used in compact, field-deployable designs [12,13].

This paper presents a proof-of-concept, microcontroller-based micro-volume spectrophotometer, which explores a framework to potentially fill the gap of an absolutely portable, inexpensive, and intelligent analytical instrument to provide real-time concentration estimates in a wide range of resource-limited settings. It is a low-cost, 8–15 µL device inspired by high-precision micro-volume spectrophotometers, like ThermoScientific NanoDrop, which are highly regarded in terms of functionality, but are prohibitively expensive.

The SPPM 3.3 is optimized in its functionality by an optoelectronic design which includes a multi-wavelength illumination module, with simple light detection and several processing levels. It provides a compact, lightweight performance in a streamlined architecture housed in a 3D printed body [14,15]. Strong spectral reconstruction is achieved by using advanced interpolation methods like piecewise cubic Hermite interpolating polynomial (PCHIP), complemented with a case-specific lightweight neural network. These approaches highlight important trade-offs between cost and spectral coverage, underscoring the need for system-level optimization. The proposed spectrophotometer's analytical performance is tested against a standard bovine serum albumin (BSA) test via the Biuret assay, a well-characterized and widely used protein estimation standard, with a commercial JENWAY 6305 spectrophotometer, considered an industry standard with high scanning speed and reliable performance. The study is a step in democratizing portable analytical instrumentation, providing an extendable framework for cost-effective and portable, micro-volume analysis demonstrated with BSA protein quantification as a representative case study.

2. Materials and methods

This section details the hardware and software considerations in designing the system. The hardware consists of light sources, optical pathways, and a measuring platform brought to life with a rechargeable battery-operated luminous intensity sensor. The system algorithm is powered by an ARM processor with multiple carefully designed processing modes.

2.1. System design

The proof-of-concept system consists of a light source assembly including two LEDs for measurements in the UV and visible region (375 nm to 700 nm), a precise measurement platform for microfluidic handling, and a detection unit employing the TSL 2561 luminous intensity sensor [16,17]. A 3.5-inch OLED screen and push buttons allow interactive feedback and data visualization. The device is powered by a rechargeable 3.7V LiPo battery [17,18]. The entire system is housed in a 3D-printed modular body, fabricated using polylactic acid (PLA) via fused deposition modeling (FDM). The overall workflow of the proposed micro-volume spectrophotometer (SPPM3.3) is illustrated in Figure 1.

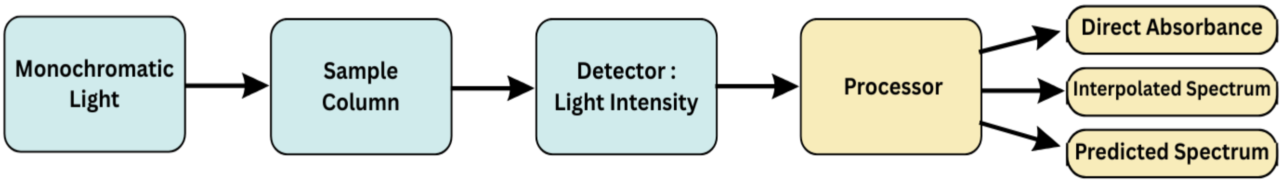

Figure 1. System workflow diagram.

The LED is being used as a reliable light source in the portable device [12,13] alongside conventional xenon, deuterium, and tungsten lamps due to its effective and consistent long-term light while maintaining a short warm-up time [12,19]. Its semi-chromatic character provides a narrow spectral range, reducing the need for monochromators; although parasitic spectral emissions are commonly observed, they can be reduced via filtration [12,19]. To minimize the influence of power supply noise and temperature fluctuations, the LEDs were powered at a constant voltage of 5V and switched only during measurement.

Figure 2 illustrates the optical path for the micro-volume chamber of the device. The source emits light which is directed through a beam splitter with two inputs: the UV LED and the RGB module. The beam, falling at a 0° incidence angle is directed through a collimating lens, the sample placed between two glass slides, and a second collimating lens before reaching the detector. Glass was chosen to interact with the light because of its high UV-visible transmittance and good thermal and chemical resilience which is well illustrated in microfluidic and bio-sensing systems [20,21]. Collimating lenses ensure that focused light reaches the detector after signal losses customary to redirection by the optical splitter [20].

A meticulously calibrated measurement platform hosts 8–15 µL of sample and forms a sample column of approximately 2 mm above the detector to ensure maximum interaction with incident light. This column is created with the aid of springs on either side of the stage that recoil after glass slides make contact with the sample upon closure. The liquid's surface tension ensures a stable meniscus between the slides that keeps the optical path intact and holds the volume of the sample in place during measurement. The optical setup and component placement is fixed with the enclosure geometry to maintain consistent alignment between the light source, sample region and detector.

Technological advancements [12,19] have made CCDs and photodiodes a reliable choice for low-cost analytical systems. These detectors are small, efficient, and offer a large linear range of response with low noise. The TSL 2561 sensor used in this system is based on two photodiodes and a 16-bit ADC offering a wide, non-selective, near-phototropic response in the 300 to 700 nm range [16]. The sensor, powered by a rechargeable 3.7 V LiPo battery, measures the intensity of incoming light and sends the data to an ARM processor for further processing. Similar to most available designs [18,22], the system algorithm assesses the absorbance of selected wavelengths and outputs their value based on the transmittance of light.

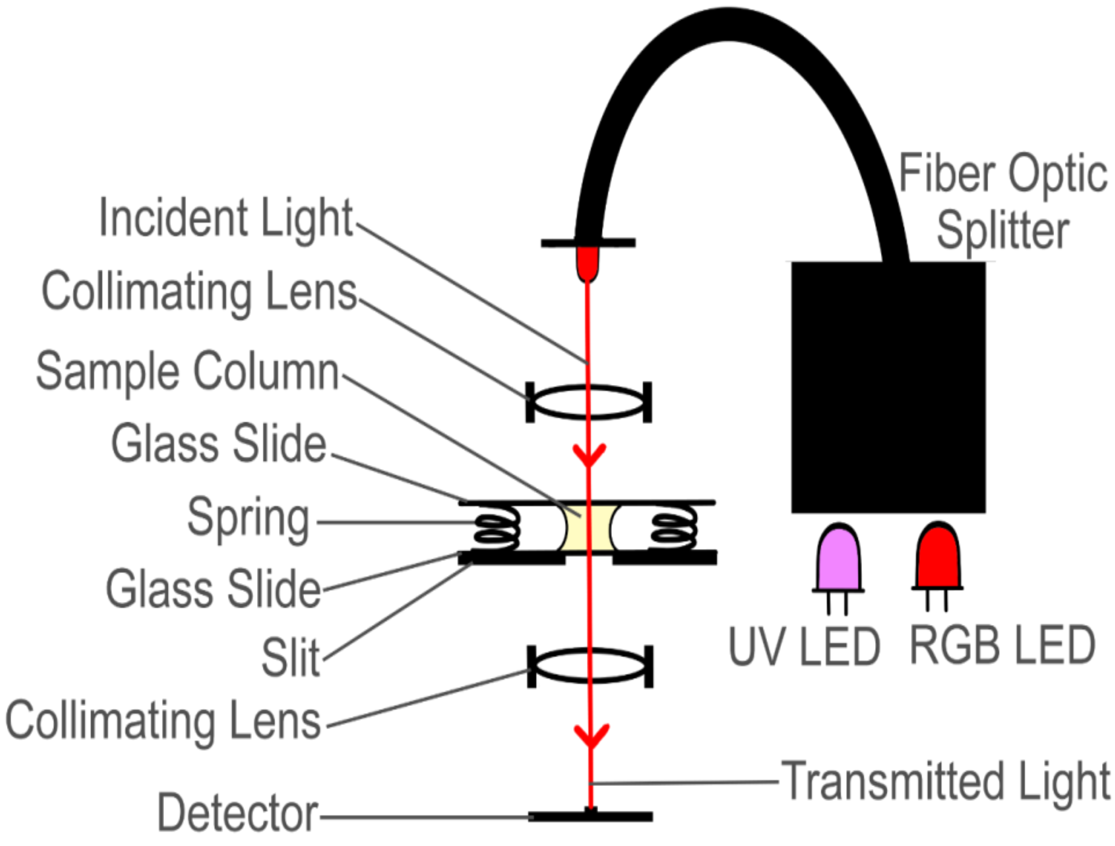

Figure 2. Optical Path assembly with light sources, beam splitter, lenses, sample chamber and detector. The glass slides maintain a 2 mm sample column via spring-loaded compression.

2.2. System algorithms

The system's algorithm implements three distinct processing modes illustrated in Figure 3. The user may choose to obtain the absorbance value of any one of 4 available wavelengths in the direct absorbance mode or generate an absorbance spectrum using interpolation or a case-specific neural network, both based on measurements from four data points. Once selected, the algorithm generates appropriate prompts guiding the user through each step.

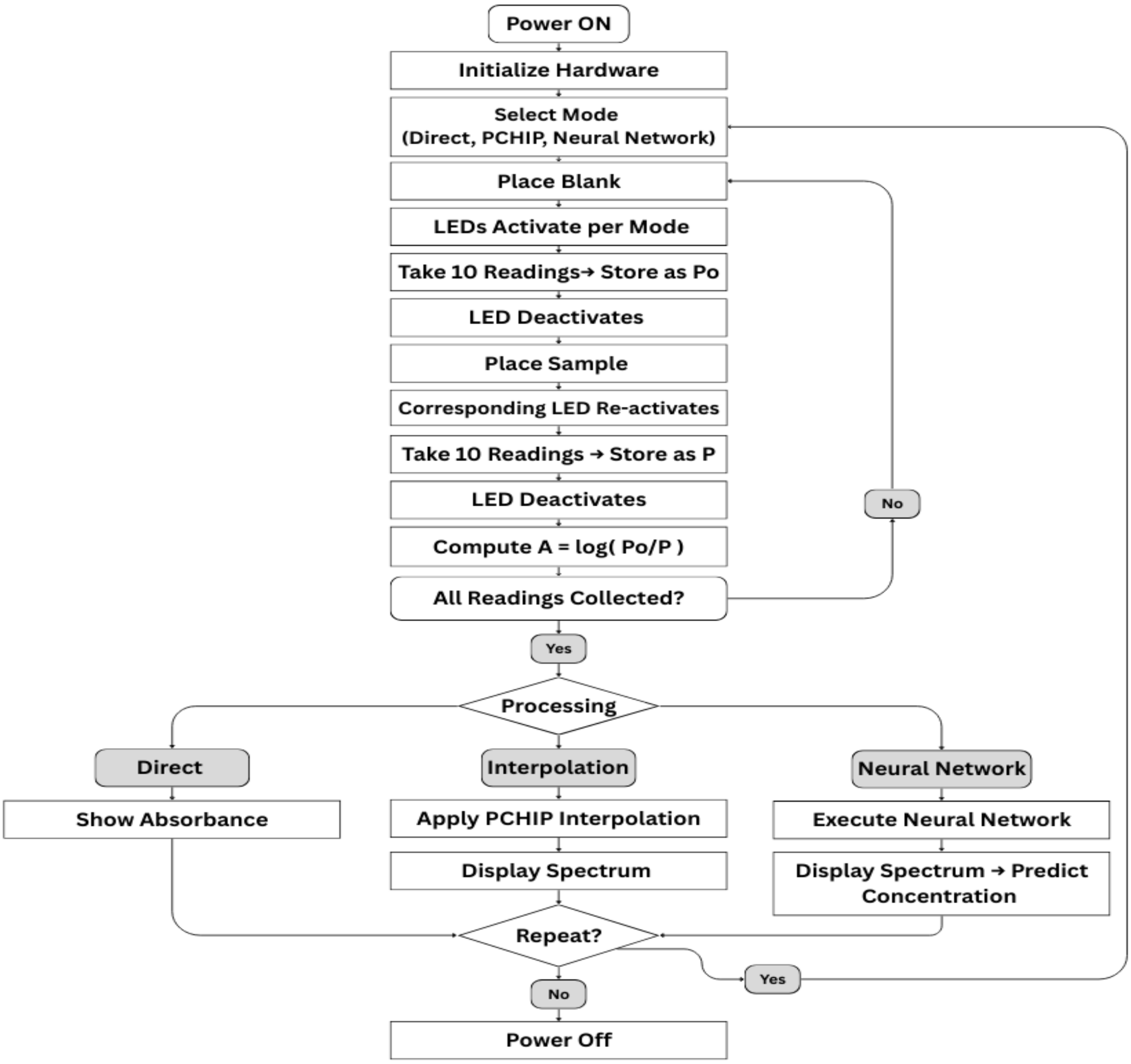

Figure 3. System algorithm detailing three distinct processing modes.

In the direct absorbance mode, light intensity readings for each sample are used to calculate absorbance based on the Beer-Lambert law [23]. The relationship between absorbance, concentration and measured intensities is expressed by the following equation.

$$A=\varepsilon cl=log_{10}\left(\frac{P_0}{P}\right) \tag{1}$$

Here, A is the absorbance of the solution, ε is the molecular absorptivity, c is the concentration, and l is the path length, which is set to 2 mm in this device, otherwise 10mm in standard cuvette-based operations [24]. This device calculates absorbance using measured light intensities, where P_0, is the magnitude of transmitted light through the reference, a blank consisting of distilled water, and P is the magnitude of transmitted light through the sample.

The interpolated spectrum mode implements a PCHIP to reconstruct a continuous absorbance spectrum using absorbance at 4 known points computed using equation 1. A smooth, shape-preserving curve is produced by calculating localized cubic Hermite polynomials that pass through each known pair of points while preserving monotonicity and controlling overshoots [25]. 13 absorbance values are obtained in the wavelength range 375 to 700 nm based on the algorithm proposed by Fritsch and Carlson (1980) [26], where interval slopes are computed by:

$$\delta_i = \frac{y_{i+1} - y_i}{x_{i+1} - x_i} \tag{2}$$

Where known absorbance values y_i, y_{i+1} at wavelengths x_i, x_{i+1}
Monotonicity-preserving formulas are used to derive pointwise derivatives, mi which are then used to interpolate absorbance at target wavelengths $x \in [x_i, x_{i+1}]$ using the Hermite cubic formula:

$$H(t) = h_{00}(t) y_i + h_{10}(t) h_i m_i + h_{01}(t) y_{i+1} + h_{11}(t) h_i m_{i+1} \tag{3}$$

$$\text{Where } t = \frac{x - x_i}{x_{i+1} - x_i} \text{ and } h_{00}, h_{01}, h_{10}, \text{ and } h_{11} \text{ are Hermite basis functions.} \tag{4}$$

Unlike traditional cubic spline or linear interpolation, PCHIP is specifically designed to preserve the shape and monotonicity of complex data, avoiding overshoots and unrealistic oscillations, resulting in smooth output curves close to reference curves [25].

A continuous absorbance spectrum is obtained using an embedded neural network, designed using tiny ML techniques [27,28]. Feedforward neural networks, particularly when trained using the Levenberg–Marquardt algorithm [29], have demonstrated strong capability in modeling nonlinear systems with high efficiency and precision. Small-scale NN architectures have proven their effectiveness in low-power, embedded TinyML implementations. In recent times, an increase in exploration of NN has been observed in spectrum prediction for spectroscopy [30,31].

This mode is specific to the quantification of BSA, with a feedforward neural network trained on a limited dataset of BSA concentration [32,33] measured via the biuret assay. This compact model was trained via the Marquardt algorithm [29,34] and exported to the ARM processor with its weights and biases. The neural network implementation is application-specific, and does not generalize beyond BSA quantification without re-training under assay-specific protocols.

2.3. Machine learning model

2.3.1. Dataset acquisition

A stock solution of BSA protein was prepared at 1% (w/v), and serial dilutions were made using distilled water to obtain concentrations of 0.8%, 0.6%, 0.4%, 0.2%, and 0%. Each 2 mL sample was combined with 1 mL of Biuret reagent and mixed thoroughly to ensure homogeneity. Absorbance readings were recorded at multiple wavelengths across the UV-VIS range (375–700 nm, in 25 nm increments) using the JENWAY 6305 spectrophotometer, referred to as the Lab spectrophotometer in the coming sections. The resulting dataset comprised absorbance spectra for each concentration, forming a basis for supervised learning.

2.3.2. Neural network training

This system employs a feedforward neural network to predict the full absorbance spectrum and estimate protein concentration from four key wavelength measurements. The network consisted of a single hidden layer with six neurons using the hyperbolic tangent sigmoid activation function, enabling efficient modeling of complex spectral patterns. The architecture of the proposed neural network is shown in Figure 4.The input includes absorbance values at 375 nm (UV), 475 nm (blue), 525 nm (green), and 625 nm (red). The network was trained to output 15 values: absorbance at 14 wavelengths (375–700 nm, in 25 nm steps) and the corresponding BSA concentration.

Training was performed using the Levenberg–Marquardt algorithm [29,34] with a fixed random seed to ensure reproducibility [35]. To mitigate the risk of overfitting common to models trained on small datasets, a 5-fold cross-validation strategy was employed during development. After iterative training with subsets the average root mean square error (RMSE) across validation folds was found to be 0.028 indicating consistent predictive performance within the measured concentration range. Following cross-validation, the final deployed model was retrained using the full dataset to maximize performance within the defined domain.

The deployed model contained 135 parameters with 24 input weights (4 inputs × 6 hidden neurons), 6 hidden biases, 90 output weights (15 outputs × 6 hidden neurons), and 15 output biases. Once trained, these parameters were extracted and converted into microcontroller-compatible arrays. The complete neural network was embedded as a lightweight function, enabling real time spectrum reconstruction and BSA concentration prediction directly on the microcontroller, facilitated by a mere 2KB of RAM.

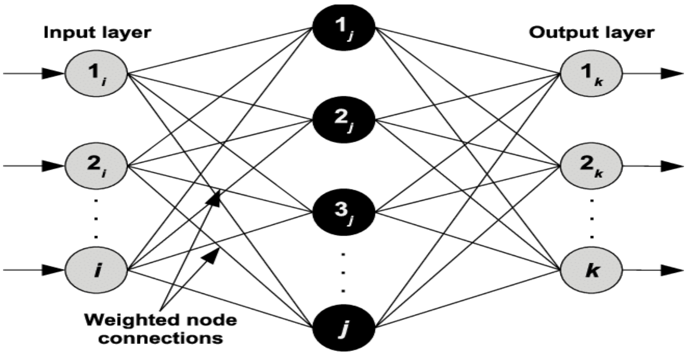

Figure 4. Structure of a single layer feed-forward neural network.

3. Results and discussion

The meticulous component selection ensured that only widely available, off the shelf components are used, along with additively manufactured structural parts for ease of replication in resource-constrained areas. The total cost of all components comes to $35.79. This cost reflects prototype level procurement, summarized in Table 1. Compared to low-cost solutions in cuvette-based spectroscopy coming up to $50 [18,22] and above, with commercial micro-volume alternatives costing between $2000 to $10,000, the SPPM3.3 establishes itself as a cost-effective design. The fully assembled SPPM3.3 prototype is shown in Figure 5.

Table 1. Summarized bill of materials.

Component	Cost (USD)
Light sources	0.25
Optical path assembly	11.29
TSL2561 luminous intensity sensor	2.14
Microcontroller unit	2.32
Power supply and regulation	2.21
OLED display	1.25
3D printing – enclosure	12.50
Miscellaneous electronics	3.83
Total	35.79

Figure 5. Labelled diagram of fully assembled SPPM3.3 prototype.

3.1. Absorbance trends and calibration

The absorbance spectrum comparison between the reference (LAB) and prototype (SPPM 3.3) (Figure 6) shows that SPPM 3.3 closely follows the lab instrument's trend, matching best in the blue range (475 nm). Minor deviations at 525 nm and 625 nm appear as expected artifacts, such as the lack of true monochromaticity, causing the occasional stray light effect in prototype optical systems [12,19,35]. The comparative analysis between the Lab and SPPM readings of BSA indicates good overall agreement on the basis of RMSE and R^2 score discussed in the sections below. Potential causes of minor systematic bias observed in Bland-Altman analysis can be explained by signal losses in optical splitting, commonly noted in similar redirection efforts [20,21]. All comparisons illustrated in plots are performed against the JENWAY 6305, a cuvette-based laboratory spectrophotometer at representative BSA concentrations to evaluate overall trend fidelity.

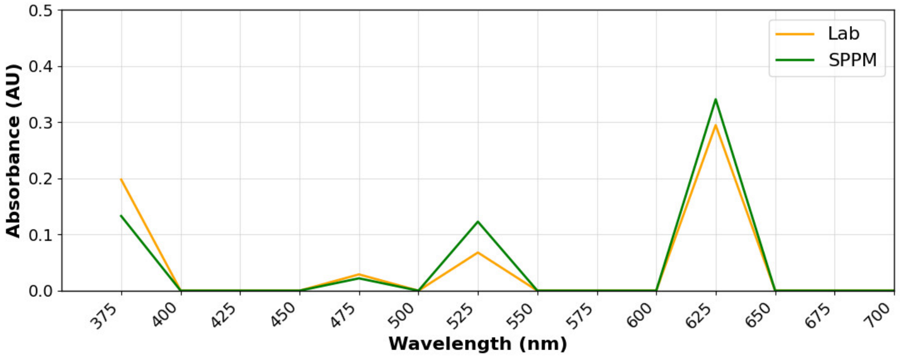

Figure 6. Comparative absorbance spectrum between the reference (LAB) and SPPM3.3 for a representative BSA sample. Absorbance values correspond to discrete wavelength measurements in the 375–700nm range, illustrating spectral trend agreement rather than absolute analytical equivalence. The numerical dataset used to generate this figure is provided in the Supplementary Material (Table S1).

3.2. Interpolation accuracy

The PCHIP-based spectral reconstruction follows the general reference spectrum, illustrating its shape-preserving characteristics, as illustrated in Figure 7. Overshoots are significantly mitigated while preserving the shape more closely in comparison to cubic spline interpolation [25]. It must be noted that the severe deflection towards the end of the graph, while significantly reduced by the PCHIP technique, influences overall results. This is due to the PCHIP technique's reliance on gradients between data points for accurate calculations, as detailed in the system algorithm [26]. The boundary past 625 nm is left undefined, and therefore, values calculated in that range (650–700 nm) contain discrepancies.

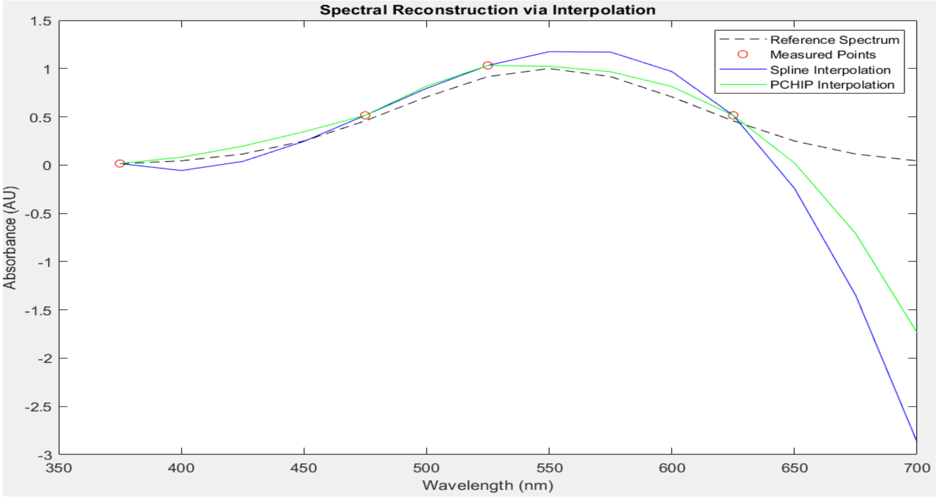

Figure 7. Comparison of cubic spline and PCHIP interpolation methods for spectral reconstruction using four discrete absorbance measurements (375, 475, 525, 625 nm) against reference spectrum. PCHIP interpolation demonstrates reduced overshoot behavior in unbounded conditions (>625 nm) compared to cubic spline interpolation.

The reconstructed absorbance spectrum generated using PCHIP interpolation and its comparison with the laboratory reference spectrum are illustrated in Figure 8. Error and R2 score calculations further fortify this observation. Deflection from the reference in Figure 8 was studied, and the last two readings at wavelengths 675 and 700nm were excluded from quantitative error metrics, as they lie outside the bounded interpolation region defined by the measured data points. This resulted in a decrease in RMSE from 0.087 to 0.032 AU with a significant increase in R^2 score from 0.517 to 0.908 for the lab readings, proving the reliability of the PCHIP interpolation technique within a bounded range. Similarly, for SPPM3.3 readings, the RMSE decreased from 0.077 to 0.037 AU while the R^2 score improves from 0.592 to 0.792.

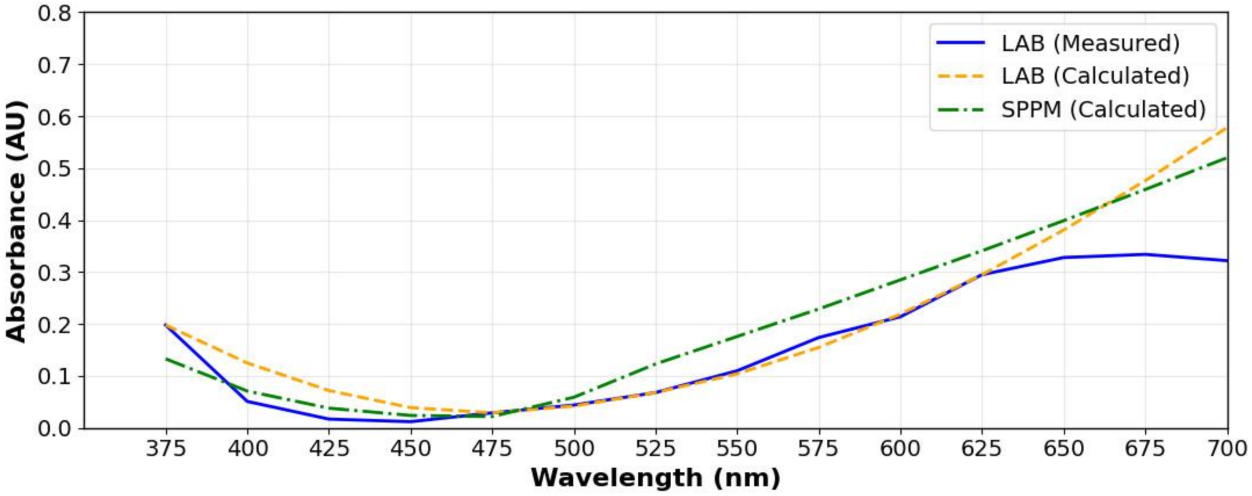

Figure 8. Reconstructed absorbance spectrum using PCHIP interpolation compared to the reference spectrum (LAB [measured]) for a representative BSA sample. Interpolated values spanning 375–625 nm using 4 discrete measurements (375, 475, 525, 625 nm). Deviation observed beyond 625 nm reflects unbounded extrapolation. The numerical dataset used to generate this figure is provided in the Supplementary Material (Table S2).

Figure 9 presents an overlay Bland–Altman plot [36,37] comparing the calculated SPPM3.3 and laboratory absorbance values against the reference spectrum. The analysis shows an expected minor systematic bias of 0.0300 and 0.0156, respectively. While most points occur well within the limits of agreement (LOA) region, one point from the SPPM3.3 appears outside the 95% confidence interval. Together with the R^2 score, the technique demonstrates acceptable agreement. A minor systematic over-estimation is observed, which is consistent with other LED-based spectrophotometers, [18,22] discussed previously.

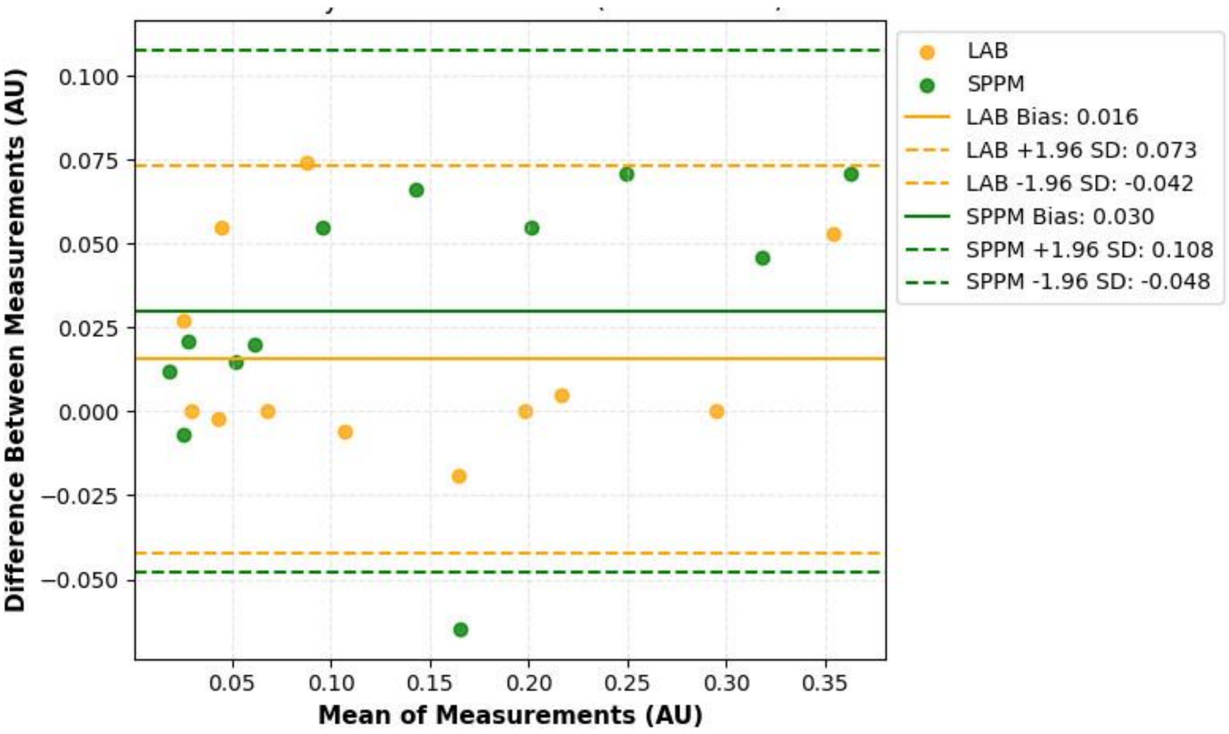

Figure 9. Bland-Altman analysis comparing PCHIP-interpolated absorbance values from reference (Lab) and SPPM3.3 measurements. Dashed lines indicate 95% limits of agreement with data points within bounded interpolation range (375–650 nm). The numerical dataset used to generate this figure is provided in the Supplementary Material (Table S2).

3.3. Neural network performance

Figure 10 shows the reconstructed absorbance spectrum predicted by the neural network model compared with the laboratory-measured reference spectrum for a representative BSA sample. The neural network establishes its reliability with R^2 scores of 0.982 and 0.909 for the Lab spectrophotometer and SPPM3.3, respectively. This shows a close reconstruction of the spectrum, which is predicted adequately by the SPPM curve in Figure 10. The network models longer wavelengths more smoothly, while hiccups are observed among shorter ones. The model has learnt the data considerably well, as demonstrated by the Lab curve with a small RMSE of 0.016 absorbance units. The SPPM3.3 curve, however, requires improvement. While the R^2 score proves a general reliability, over and underestimates can be seen in the shorter wavelength region with an RMSE of 0.036 absorbance units. The curve modelling remains imperfect; however, the network successfully predicts accurate concentration values within the trained concentration range.

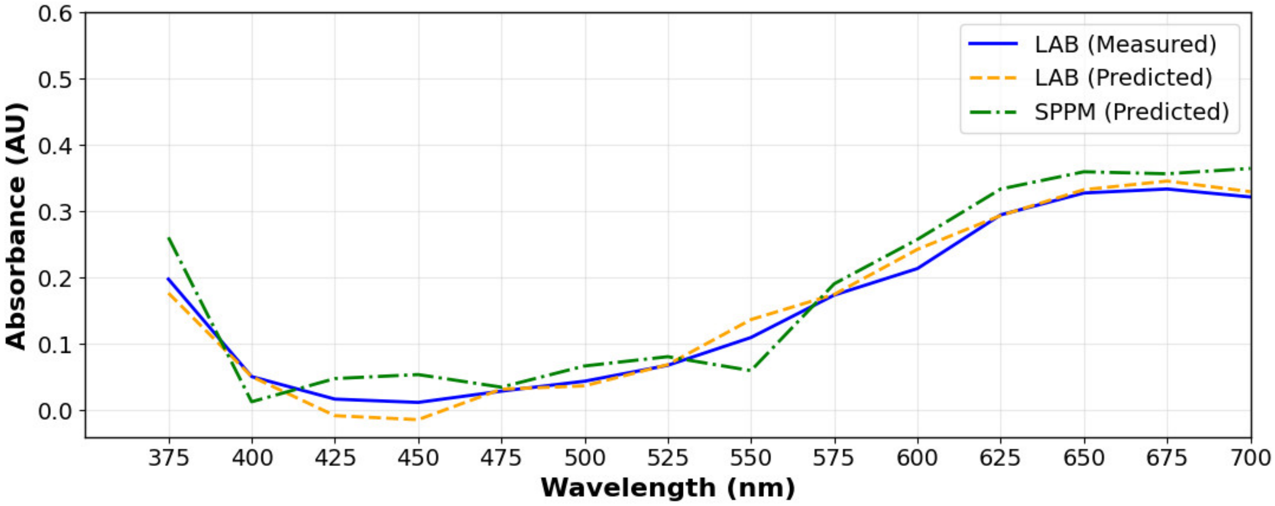

Figure 10. Reconstructed absorbance spectrum using feedforward neural network (6 hidden neurons, hyperbolic tangent activation) trained on BSA calibration dataset is compared to reference spectrum (LAB [measured]) for a representative BSA sample. Predicted values span 375–700 nm using 4 discrete measurements (375, 475, 525, 625 nm) as input. The numerical dataset and machine learning specifications for this figure are provided in the Supplementary Material (Table S3 and S4).

Figure 11 presents an overlay Bland-Altman [36,37] plot comparing neural network–predicted absorbance values from SPPM3.3 and laboratory measurements against the reference spectrum. The analysis shows a minor systematic bias of 0.0206 and 0.0004, respectively. While most points occur well within the LOA region, two points from the SPPM appear close to the LOA, with one outside of the 95% confidence interval, primarily at shorter wavelengths where LED spectral bandwidth and detector sensitivity impose higher uncertainty The points are spread on either side of the bias, not indicative of clear overfitting, the risk of which was mitigated by cross-fold validation during training (discussed previously in section 2.3.2). Overall, the technique demonstrates stable agreement within the evaluated operating range, in comparison with R^2 scores and RMSE of neural network-based studies [30,31].

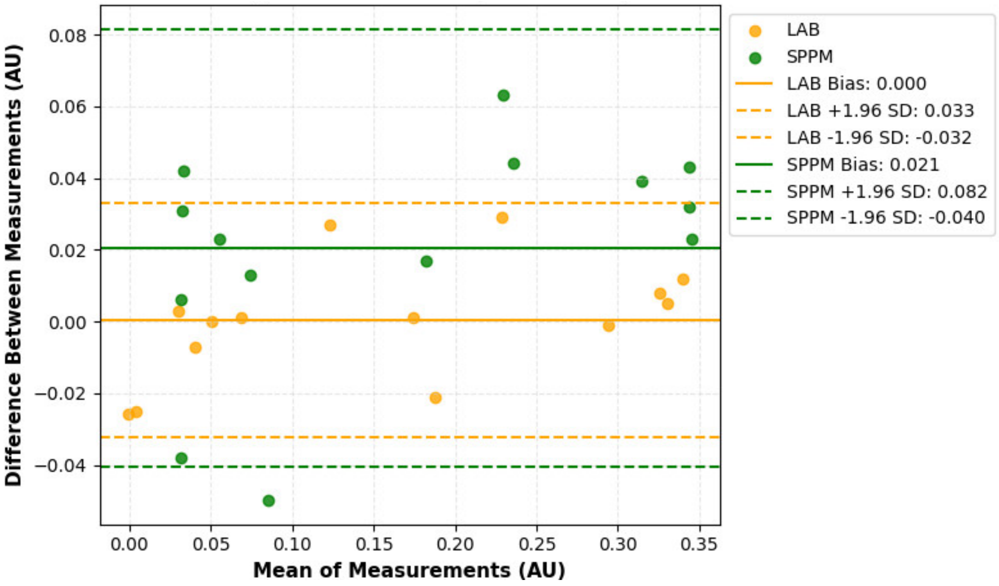

Figure 11. Bland-Altman analysis comparing neural network-predicted absorbance values from reference (Lab) and SPPM3.3 measurements. Dashed lines indicate 95% limits of agreement across full reconstruction range (375–700 nm). The numerical dataset used to generate this figure is provided in the Supplementary Material (Table S3).

3.4. Comparative analysis of processing techniques

A quantitative comparison based on Table 2 concludes that the neural network achieves lower RMSE and higher R^2 score than PCHIP based reconstruction for the evaluated dataset. This numerical difference is not interpreted as inherent superiority of one technique over the other due to fundamental differences in their sources of information and computational formulation. The two approaches are therefore considered complementary perspectives as their trade-offs are discussed further.

The PCHIP interpolation method enforces local shape preservation and monotonicity between measured data points, resulting in smoother reconstructions within the bounded wavelength range defined by the inputs. In contrast, the neural network uses learned relationships from intermediate spectral values present in the training data, enabling reconstruction based on nonlinear trends which are not explicitly encoded in gradient-based interpolation. This distinction is particularly relevant near spectral boundaries and unbounded domains where interpolation is more sensitive to gradient behavior, while a data-driven approach depends on training data representativeness.

Direct performance comparison with caution; however, a key takeaway is that both techniques would benefit from increased input data density through additional wavelength sampling or expanded training datasets while adhering to hardware and software limitations of portable low-cost devices, such as storage space and component restrictions [28]. The minor systematic bias that is observed in both techniques is common to LED-based spectrophotometers [18,22] and optical redirection setups [20] and therefore remain acceptable in light of comparable RMSE and R^2 scores in studies involving more complex techniques and computation, such as recurrent and convolutional neural networks (RNN and CNN), [30,31] and cuvette-based LED spectrophotometers [18,22]. Future work will focus on extending this analysis across additional analytes and operating conditions to further characterize these trade-offs.

Table 2. RMSE and R^2 values comparing PCHIP interpolation and neural network based spectral reconstruction of lab data vs SPPM for representative BSA samples.

	Interpolation via PCHIP	Prediction via neural network
RMSE (LAB) (AU)	0.0322	0.0160
RMSE (SPPM) (AU)	0.0484	0.0364
R2 score (LAB)	0.9075	0.9823
R2 score (SPPM)	0.7916	0.9089

3.5. System level interpretation and validation scope

The results presented in the previous sections reflect the performance of the SPPM 3.3 as an integrated spectrophotometric system, where optical configuration, enclosure geometry, sensing hardware, and signal processing jointly influence measurement outcomes. Reconstruction accuracy and observed biases are therefore interpreted in the context of the complete measurement pipeline instead of isolated properties of the processing algorithms. Measurement uncertainty arises from multiple optical and electronic sources, including LED spectral bandwidth [8], optical splitting losses [20,21], and detector sensitivity, which contribute to systematic bias and variance especially at shorter wavelengths where low photodiode efficiency results in lower signal to noise ratio.

The optical layout and enclosure ensure fixed alignment between the light source, sample region, and detector while prioritizing controlled optical pathways within a compact form factor. The measurement chamber is enclosed for minimal ambient light interference, and the fixed optical assembly reduces alignment variability due to repeated handling. These design choices, inspired by other 3D-printed micro-fluidic devices [12,19,35] do not imply quantified repeatability or long-term robustness testing, but rather provide a framework for a structurally stable platform suitable for controlled, proof-of-concept evaluation. Minor systematic deviations observed in interpolation and neural network reconstruction are consistent with expected behavior in LED-based systems and light redirection systems, as reported in related low-cost spectrophotometric designs.

Experimental evaluation was conducted using a well-established standard for protein quantification, BSA in the Biuret assay with standard calibration and control protocols, such as blank measurements with distilled water, controlled laboratory settings, and triplicate readings. The use of BSA provides a representative and interpretable test case for assessing absorbance trends, spectral reconstruction behavior, and concentration estimation in a micro-volume context. Furthermore, the test case allowed algorithm stability evaluation sufficient for preliminary validation of a proof-of-concept setup without exhaustive analytical characterization. Within this defined scope, performance metrics, including limit of detection and quantification, linear dynamic range and formal repeatability tests were not systematically characterized. However, the proposed system demonstrates meaningful agreement with reference cuvette-based spectrophotometer (JENWAY 6305). For a proof-of-concept device intended for preliminary screening and point-of-care applications in resource-limited settings, the observed agreement (R^2 >0.9, systematic bias <0.03 AU) represents acceptable initial performance within the prototype scope. This supports its role as an extendable functional framework through appropriate calibration, assay-specific protocols, and model retraining.

Collectively, the presented results establish preliminary system-level validation of the proposed architecture. Direct comparative evaluation with commercial micro-volume systems, such as the ThermoScientific NanoDrop, represents the next step alongside pathways for extension, including increased wavelength sampling density, and robust, long-term stability and performance assessment under varied operating conditions.

4. Conclusion

This work presents a proof-of-concept, low-cost, micro-volume spectrophotometer exploring compact optical measurement and embedded spectral reconstruction under resource constraints. Using the BSA quantified via the Biuret assay as a representative standard for protein quantification, the system demonstrates consistent absorbance trend agreement with a laboratory cuvette-based spectrophotometer. Two complementary processing approaches were studied, a shape preserving PCHIP interpolation and a case-specific, lightweight neural network for reconstruction of absorbance spectra using limited absorbance measurements. This study focuses on highlighting the trade-offs between gradient based interpolation and data-driven, learning based predictions to provide an extendable framework for low-cost, micro-volume spectrophotometric systems prioritizing replication feasibility, efficiency, and portability.

The validation results are modestly scoped to representative concentrations and a single assay reflecting the exploratory nature of the study. Future work will focus on extending wavelength sampling density, handling of viscous and more concentrated samples and direct comparison with established micro-volume spectrophotometers alongside expanded analyte studies and robust, long-term validation. Collectively, this work establishes a flexible framework for portable, low-cost, micro-volume spectroscopy that can be systematically extended and refined to improve accessibility to analytical instrumentation in resource-constrained environments.

Use of AI tools declaration

The authors acknowledge the use of AI based language tools (Chat GPT, Claude AI, Grammarly) solely for grammar refinement, and sentence polishing. All research design, experiments, data analysis, and conclusions are the author's own.

Conflict of interest

The authors declare no conflict of interest.

Author contributions

Abia Moiz: Design, Methodology, Formal Analysis, Writing. Ayesha Faiz Ur Rasool: Design, Methodology, Data collection, Validation, Writing. Muhammad Aamir: Design, Supervision, Review & Editing. Irfan A. Usmani: Validation, Supervision, Review & Editing.

References

1. Understanding Cuvette Volume, Material, Path Length Etc. | Cuvet.Co Cells. Available from: https://cuvet.co/understanding-cuvette-volume-material-path-length-etc/.
2. Jenway 73 series. Available from: https://www.wolflabs.co.uk/documents/Jenway_Spectrophotometers_73_Series.pdf?srsltid=AfmBOop3NWKNA6mA3mWQbxVjAQP_OXzPlVKdV_OwQmMYOoiR2CyduyKv&.
3. Desjardins P and Conklin D (2010) NanoDrop microvolume quantitation of nucleic acids. *J Vis Exp* 45: e2565. https://doi.org/10.3791/2565
4. NanoDrop One Microvolume UV-Vis Spectrophotometers. Available from: https://documents.thermofisher.com/TFS-Assets/CAD/Specification-Sheets/NanoDrop-One-Specifications.pdf.
5. Minhas-Khan A, Ghafar-Zadeh M, Shaffaf T, et al. (2021) UV-Vis spectrophotometric analysis of DNA retrieval for DNA storage applications. *Actuators* 10: 246. https://doi.org/10.3390/act10100246
6. Duma Z, Ramsuran V, Chuturgoon AA, et al. (2022) Evaluation of various alternative economical and high throughput SARS-CoV-2 testing methods within resource-limited settings. *Int J Mol Sci* 23: 14350. https://doi.org/10.3390/ijms232214350
7. Desjardins P, Hansen JB, Allen M (2009) Microvolume protein concentration determination using the NanoDrop 2000c spectrophotometer. *J Vis Exp*. https://doi.org/10.3791/1610
8. Baker A, Ward D, Lieten SH, et al. (2004) Measurement of protein-like fluorescence in river and waste water using a handheld spectrophotometer. *Water Res* 38: 2934–2938. https://doi.org/10.1016/j.watres.2004.04.023
9. Di Nonno S and Ulber R (2021) Smartphone-based optical analysis systems. *Analyst* 146: 2749–2768. https://doi.org/10.1039/D1AN00025J
10. Koohkan R, Kaykhaii M, Sasani M, et al. (2020) Fabrication of a smartphone-based spectrophotometer and its application in monitoring concentrations of organic dyes. *ACS Omega* 5: 31450–31455. https://doi.org/10.1021/acsomega.0c05123
11. Aksoy S, Dulda A, Ertaş G (2023) Emerging technologies for fluorescence-based optical test strip readers. *Avrupa Bilim ve Teknoloji Dergisi* 49: 16–24. https://doi.org/10.31590/ejosat.1265098
12. Lebanov L, Mikhail IE, Paull B (2024) Light-emitting diode-based absorbance detectors for flow-through analysis in analytical chemistry: a tutorial. *J Chromatogr Open* 6: 100191. https://doi.org/10.1016/j.jcoa.2024.100191
13. Bui DA and Hauser PC (2015) Analytical devices based on light-emitting diodes – a review of the state-of-the-art. *Anal Chim Acta* 853: 46–58. https://doi.org/10.1016/j.aca.2014.09.044
14. Zhang C, Bills BJ, Manicke NE (2017) Rapid prototyping using 3D printing in bioanalytical research. *Bioanalysis* 9: 329–331. https://doi.org/10.4155/bio-2016-0293
15. Niculescu AG, Chircov C, Bîrcă AC, et al. (2021) Fabrication and applications of microfluidic devices: a review. *Int J Mol Sci* 22: 2011. https://doi.org/10.3390/ijms22042011
16. TSL2561 DataSheet. Available from: https://cdn-shop.adafruit.com/datasheets/TSL2561.pdf.
17. Chaianantakul N, Wutthi K, Kamput N, et al. (2018) Development of mini-spectrophotometer for determination of plasma glucose. *Spectrochim Acta A Mol Biomol Spectrosc* 204: 670–676. https://doi.org/10.1016/j.saa.2018.06.107

18. González-Morales D, Valencia A, Díaz-Nuñez A, et al. (2020) Development of a low-cost UV-Vis spectrophotometer and its application for the detection of mercuric ions assisted by chemosensors. *Sensors* 20: 906. https://doi.org/10.3390/s20030906
19. Macka M, Piasecki T, Dasgupta PK (2014) Light-emitting diodes for analytical chemistry. *Annu Rev Anal Chem* 7: 183–207. https://doi.org/10.1146/annurev-anchem-071213-020059
20. Keiser G, Xiong F, Cui Y, et al. (2014) Review of diverse optical fibers used in biomedical research and clinical practice. *J Biomed Opt* 19: 080902. https://doi.org/10.1117/1.jbo.19.8.080902
21. Shakeri A, Jarad NA, Leung A, et al. (2019) Biofunctionalization of glass- and paper-based microfluidic devices: a review. *Adv Mater Interfaces* 6: 1900940. https://doi.org/10.1002/admi.201900940
22. Prairie MW, Frisbie SH, Rao KK, et al. (2020) An accurate, precise, and affordable light emitting diode spectrophotometer for drinking water and other testing with limited resources. *PLoS One* 15: e0226761. https://doi.org/10.1371/journal.pone.0226761
23. Moses Kayanda Kiteto and Cleophas Achisa Mecha (2024) Insight into the bouguer-beer-lambert law: a review. *Sustainable Chem Eng* 5: 567–587. https://doi.org/10.37256/sce.5220245325
24. Tiago MM, Higuti RT, Segura LE, et al. (2019) Versatile ultrasonic spectrometer for liquids with practical sample handling by using standard cuvettes. *IEEE Trans Ultrason Ferroelectr Freq Control* 66: 109–118. https://doi.org/10.1109/TUFFC.2018.2875872
25. Rabbath CA and Corriveau D (2019) A comparison of piecewise cubic hermite interpolating polynomials, cubic splines and piecewise linear functions for the approximation of projectile aerodynamics. *Def Technol* 15: 741–757. https://doi.org/10.1016/j.dt.2019.07.016
26. Fritsch FN and Carlson RE (1980) Monotone piecewise cubic interpolation. *SIAM J Numer Anal* 17: 238–246. https://doi.org/10.1137/0717021
27. Banbury C, Zhou C, Fedorov I, et al. (2021) Micronets: neural network architectures for deploying tinyml applications on commodity microcontrollers. *MLSys Proceedings* 3: 517–532. https://doi.org/10.48550/arXiv.2010.11267
28. Heydari S and Mahmoud QH (2025) Tiny machine learning and on-device inference: a survey of applications, challenges, and future directions. *Sensors* 25: 3191. https://doi.org/10.3390/s25103191
29. Hagan MT and Menhaj MB (1994) Training feedforward networks with the Marquardt algorithm. *IEEE Trans Neural Netw* 5: 989–993. https://doi.org/10.1109/72.329697
30. Rieger LH, Wilson M, Vegge T, et al. (2023) Understanding the patterns that neural networks learn from chemical spectra. *Digital Discovery* 2: 1957–1968. https://doi.org/10.1039/D3DD00203A
31. Urbina F, Batra K, Luebke KJ, et al. (2021) UV-adVISor: attention-based recurrent neural networks to predict UV-Vis spectra. *Anal Chem* 93: 16076–16085. https://doi.org/10.1021/acs.analchem.1c03741
32. Doumas BT (1975) Standards for total serum protein assays--a collaborative study. *Clin Chem* 21: 1159–1166. https://doi.org/10.1093/CLINCHEM%2F21.8.1159
33. Noble JE, Knight AE, Reason AJ, et al. (2007) A comparison of protein quantitation assays for biopharmaceutical applications. *Mol Biotechnol* 37: 99–111. https://doi.org/10.1007/s12033-007-0038-9

34. Train Deep Neural Networks - MATLAB & Simulink. Available from: https://in.mathworks.com/help/deeplearning/train-deep-neural-networks.html?s_tid=CRUX_topnav.
35. Suhendar H, Silambi MS, Pratama MR (2024) Design of a Portable Spectrophotometer Based on Raspberry Pi for Tea Type Classification Using Machine Learning. *J Phys Conf Ser* 2866: 012041. https://doi.org/10.1088/1742-6596/2866/1/012041
36. Giavarina D (2015) Understanding bland altman analysis. *Biochem Med (Zagreb)* 25: 141–151. https://doi.org/10.11613/bm.2015.015
37. Altman DG and Bland JM (2017) Assessing agreement between methods of measurement. *Clin Chem* 63: 1653–1654. https://doi.org/10.1373/clinchem.2016.268870

AIMS Press

© 2026 the Author(s), licensee AIMS Press. This is an open access article distributed under the terms of the Creative Commons Attribution License (https://creativecommons.org/licenses/by/4.0)